

# Measurement of gas-phase hydroperoxides by chemical ionization mass spectrometry (CIMS)

John D. Crounse\*, Karena A. McKinney<sup>+&</sup>, Alan J. Kwan<sup>#</sup>, and Paul O. Wennberg<sup>+&</sup>

\*Div. of Chemistry and Chemical Engineering, California Institute of Technology

<sup>+</sup> Div. of Geological and Planetary Sciences, California Institute of Technology

<sup>#</sup> Div. of Engineering and Applied Science, California Institute of Technology

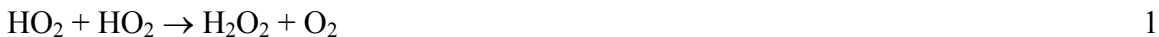
<sup>&</sup>Currently with Dept. of Chemistry, Amherst College

**Abstract.** A new method for the detection of gas-phase hydroperoxides is described. The clustering chemistry of  $\text{CF}_3\text{O}^-$  is exploited to produce speciated measurements of several hydroperoxides with high sensitivity and fast time response. Correspondence of airborne observations made with this technique and the established HPLC method is illustrated.  $\text{CF}_3\text{O}^-$  appears to be a highly versatile reagent ion for measurements of both weak and strong acids in the atmosphere.

## 1. Introduction

Hydroperoxides ( $\text{ROOH}$ ) are important components of the Earth's atmosphere. Depending on the nature of R, they have widely varying atmospheric lifetimes and impacts. In general, the larger and less polar organic hydroperoxides (e.g.,  $\text{R} = \text{CH}_3$  or  $\text{CH}_3\text{CH}_2$ ) can be transported by atmospheric motion without significant loss to cloud. Thus, these compounds serve as reservoirs of  $\text{HO}_x$  ( $\text{OH}$  and  $\text{HO}_2$ ) whose subsequent photochemistry (photolysis or oxidation by  $\text{OH}$ ) can release radicals, oftentimes in areas distant from where they are initially formed. Such transport, for example, to the upper troposphere, can significantly alter gas-phase oxidation rates and radical budgets.<sup>1,2</sup> Peroxides with high solubility (e.g.  $\text{R}=\text{H}$ ,  $\text{HOCH}_2$ ) are often lost by uptake onto aerosol and cloud droplets where they promote heterogeneous oxidation of many compounds such as  $\text{SO}_2$ <sup>3</sup> and may play a role in the formation of secondary organic aerosol.<sup>4</sup>

Hydrogen peroxide,  $\text{H}_2\text{O}_2$ , is formed in the atmosphere almost exclusively through the self reaction of  $\text{HO}_2$ :

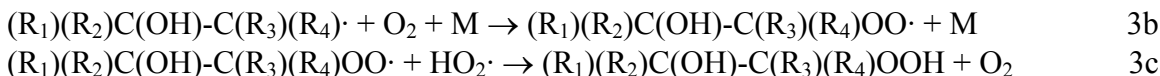


Organic peroxides generally form in the atmosphere via OH-mediated oxidation of 1) saturated hydrocarbons,



or 2) unsaturated hydrocarbons,





where R is an organic substituent (e.g. CH<sub>3</sub>), and R<sub>1</sub>-R<sub>4</sub> are either H-atom or organic substituents. Peroxides can also be produced by the ozonolysis of alkenes under high humidity conditions.<sup>5</sup> Because ROO· reacts quickly with NO, the efficiency of peroxide formation tends to decrease at high NO<sub>x</sub>, although in highly polluted environments, such as Mexico City, peroxides are predicted to be highly elevated despite the high NO<sub>x</sub> due to very high hydrocarbon concentrations.<sup>6</sup>

To date, most atmospheric peroxide measurements have required extensive sample handling.<sup>7,8</sup> Typically, sampled air is passed through water, stripping soluble peroxides into the aqueous phase. The aqueous-phase peroxides are detected using a derivatization /fluorescence technique, sometimes after separation by high performance liquid chromatography (HPLC).<sup>8-11</sup> While these methods have been tested and refined for sometime, they are limited by the solubility of ROOH, potential artifacts from aqueous phase chemistry, and the ability to separate and preserve ROOH on the HPLC column. In addition, time response can be rather long (a few minutes). Direct measurements of peroxides have been performed with tunable diode lasers, but these methods suffer from poor sensitivity and “optical noise” effects.<sup>12,13</sup>

Chemical ionization mass spectrometry (CIMS) has been shown to be a versatile and fast measurement technique for a wide variety of atmospheric trace gases. Airplane measurements by CIMS have focused on HNO<sub>3</sub>,<sup>14-20</sup> with some measurements of peroxy radicals,<sup>21</sup> SO<sub>2</sub>,<sup>16,20</sup> HCN,<sup>16,22</sup> DMSO,<sup>23</sup> OH, H<sub>2</sub>SO<sub>4</sub>, and MSA,<sup>24</sup> and ClONO<sub>2</sub> and HCl,<sup>19</sup> but the technique has also been explored for a suite of other species including CH<sub>3</sub>COOH and HCOOH,<sup>25</sup> NH<sub>3</sub>,<sup>26</sup> and HNO<sub>4</sub>,<sup>27</sup> using a wide range of ionization schemes and other conditions. For many compounds, detection limits of 10 pptv can be obtained with sub-second integration time. The fast response time allows for high temporal resolution which is particularly useful for airborne measurements.

To our knowledge, peroxides have been detected by CIMS on 3 occasions. H<sub>2</sub>O<sub>2</sub> and CH<sub>3</sub>OOH clusters with F<sup>-</sup> have been demonstrated in laboratory studies,<sup>28</sup> a cluster tentatively identified as CO<sub>3</sub><sup>-</sup>·H<sub>2</sub>O<sub>2</sub> was observed in aircraft-borne observations over Germany during a 1991 aircraft campaign aboard the DLR Falcon<sup>20</sup>, and a product ion at 101 amu was assigned to isoprene-hydroxy-hydroperoxides detected using a proton transfer reaction mass spectrometer (PTRMS) which made measurements over a tropical rainforest.<sup>29</sup> In this paper, we describe the use of the negative ion cluster chemistry of CF<sub>3</sub>O<sup>-</sup>, which has previously been shown to be useful for measurement of inorganic and organic acids,<sup>25,30,31</sup> for sensitive and selective airborne measurement of ROOH species H<sub>2</sub>O<sub>2</sub> and CH<sub>3</sub>C(O)OOH (peroxyacetic acid, PAA). We also report the results of an intercomparison between our technique and the established HPLC method<sup>11</sup> performed on the NASA DC-8 during the Intercontinental Chemical Transport Experiment – North America (INTEX-NA, summer 2004) which shows these two methods to be in good agreement.

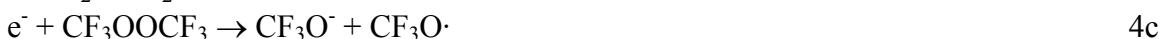
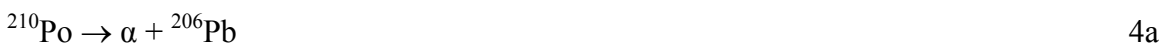
## 2. Instrument Description

The Caltech CIMS instrument was built in 1998 through a joint collaboration with the National Center for Atmospheric Research (NCAR) to measure polar stratospheric HNO<sub>3</sub> on the NASA ER2 aircraft.<sup>14</sup> It was retrofitted in 2003 to fly aboard the NASA DC-8 aircraft and the suite of compounds quantified has been broadened. The instrument components, described below, are depicted in figure 1.

Figure 1:

Ambient air is sampled through a custom, partially stopped, aluminum inlet (A and B in figure 1), which directs a fraction of the flow perpendicularly towards the instrument and serves as a virtual impactor to discriminate against particles of diameter > 0.3 μm from the sample flow. Upon redirection, the sample air flows through a glass tube (C), coated with a thin layer of Teflon © (Fluoropel PFC 801A, Cytonix Corp.) to minimize surface hydrophilicity, which is particularly problematic for HNO<sub>3</sub>. Wall effects are further mitigated because flow through the glass tube is fast (~ 40 m/s), and only the center of the flow passes through the adjustable aperture (G) into the ion flow tube (J), while the rest is exhausted through the arms of the aluminum y-block (F).

The reagent ion is produced by flowing a 10 ppm mixture of CF<sub>3</sub>OOCF<sub>3</sub> in N<sub>2</sub> at a rate of 400 standard cubic centimeters per minute (sccm) at 35 hPa total pressure through a cylindrical ion source cup (M) lined with a nickel foil containing a layer of polonium-210 and sealed with a gold coating (NRD LLC - initially 4.5 mCu activity). Polonium-210 ejects α particles which start the series of reactions leading to formation of CF<sub>3</sub>O<sup>•</sup>:



The CF<sub>3</sub>OOCF<sub>3</sub> was prepared by Dr. Darryl DesMarteau of Clemson University. Careful storage and handling of the CF<sub>3</sub>OOCF<sub>3</sub> is required to produce a clean CF<sub>3</sub>O<sup>•</sup> source. We highly recommend use of an all metal storage system. Small amounts of silicone from o-rings and grease in valves, regulators, and tubing within the gas handling system lead to unacceptably high impurity ions such as Si(CH<sub>3</sub>)<sub>3</sub>F<sub>2</sub><sup>-</sup> (m111), Si(CH<sub>3</sub>)<sub>2</sub>F<sub>3</sub><sup>-</sup> (m115), Si(CH<sub>3</sub>)F<sub>4</sub><sup>-</sup> (m119), and SiF<sub>5</sub><sup>-</sup> (m123) which presumably are ions formed from the reaction of CF<sub>3</sub>O<sup>•</sup> with fluorinated silicon molecules (Si(CH<sub>3</sub>)<sub>3</sub>F, Si(CH<sub>3</sub>)<sub>2</sub>F<sub>2</sub>, Si(CH<sub>3</sub>)F<sub>3</sub>, and SiF<sub>4</sub>, respectively). These fluorinated silicon molecules seem to form through the reaction of CF<sub>3</sub>OOCF<sub>3</sub> (or some degradation product thereof) with silicone present in the system. The removal of all silicone compounds from the system virtually eliminates these impurities.

Transport of the ions out of the source is enhanced by applying an electric potential between the source cup and the source cap (N). The cup and cap are typically held at -250 V and -240 V, respectively, with respect to the pinhole orifice plate (O). There is essentially no pressure drop between the ion source and the ion/molecule reaction region (K) in the ion flow tube (J). As the ions (K) enter the ion-molecule reaction region they are

accelerated towards the pinhole, perpendicular to the sample flow, by the electric field between the source cap and the pinhole orifice plate ( $\sim 100$  V/cm). In this region, the ions react with trace gases in the sample air to form selective product ions (described in section 3). The adjustable orifice (G) is adjusted using a computer controlled stepper motor to maintain a constant flow tube pressure ( $\sim 35$  hPa). A critical orifice (L) located just after the ion-molecule reaction region ensures a constant mass flow ( $\sim 2$  standard liters per minute) through the flow tube. Temperature throughout the flow tube is close to  $20^\circ\text{C}$ , but varies somewhat with the temperature outside the aircraft and the temperature of the aircraft cabin.

The average ion-molecule reaction time in the flow tube is approximately 1 ms. This is determined by monitoring the ratio of  $[\text{HF}\cdot\text{NO}_3^-]$  to  $[\text{CF}_3\text{O}^-]$  as a function of  $[\text{HNO}_3]$  and using the established rate constant for the reaction  $\text{HNO}_3 + \text{CF}_3\text{O}^- \rightarrow \text{HF}\cdot\text{NO}_3^- + \text{CF}_2\text{O}$ .<sup>25, 31</sup> The reaction time estimated in this manner is somewhat longer than the transit time calculated for an electric field of 100 V/cm over the flow tube diameter of 2.5 cm at 35 hPa, possibly due to the non-uniform electric field produced across the flow tube.

After formation, the product ions are sampled into the high vacuum system through a 260  $\mu\text{m}$  pinhole on the orifice plate (O). They are then directed through lens 1 (P) and enter the octopole ion guide (Q) composed of 0.635 cm diameter precision ground stainless steel rods arranged in a circle with I.D. 1.78 cm and held together by two Teflon mounting rings. The octopole power supply is a simple resonant circuit, composed of an air core transformer whose primary is driven by switching transistors. The power supply operates at  $\sim 1.2$  MHz and is tuned into resonance by adjusting the frequency. The typical RF amplitude is 200 V peak to peak. The pinhole and lens 1 are normally held at aircraft ground, while the octopole bias is set to +1.5 V to optimize ion throughput while minimizing fragmentation of weakly-bound clusters such as  $\text{CF}_3\text{O}^- \cdot \text{H}_2\text{O}_2$ . The octopole chamber is  $\sim 10^{-3}$  hPa under the typical gas load (gas flow of  $\sim 20$  sccm at a flow tube pressure of 35 hPa and temperature of  $20^\circ\text{C}$ ) by turbo pump 1 (R, Varian V-250).

As the ions exit the octopole they pass through lens 2 (S), set at +18V, into the quadrupole chamber. The quadrupole chamber is differentially pumped by a second turbo pump (Y, Varian V-250) to a pressure of  $1 \times 10^{-5}$  hPa under gas load; this turbo pump exhausts into the low pressure side of turbo pump 1 to reduce power consumption and heat production. In the quadrupole chamber, the ions pass through a series of four lenses (T-W) held at -40, +220, -100, and +30V, respectively, to focus and energetically prepare the ions for the mass filter (X), a commercial 19 mm quadrupole (Extrel). The quadrupole power supply (QSC Systems) enables selective filtering of masses ranging from 10-250 amu with unit mass resolution, and consumes  $\sim 30$  W of power. The ions of a selected mass exit the quadrupole, and are detected using a channel electron multiplier (Z, K&M 7550m) operated in pulse counting mode with a preamp/discriminator (Amptek A-101) allowing for single ion detection and count rates up to 4 MHz. All instrument control and data collection is conducted with a PC-104 computer through data acquisition boards (Diamond Systems) running a real-time operating system (QNX 4.25) using custom control software.

### 3. Ion Chemistry and Water Dependence

In the first laboratory study of  $\text{CF}_3\text{O}^-$  chemistry, Huey et al. identified fluoride ion transfer as the primary reaction pathway of  $\text{CF}_3\text{O}^-$  with strong acids, i.e.,  $\text{CF}_3\text{O}^- + \text{HX} \rightarrow \text{HF} \cdot \text{X}^- + \text{CF}_2\text{O}$ .<sup>31</sup> Amelynck et al. later showed that for weaker acids, such as  $\text{HC}(\text{O})\text{OH}$  and  $\text{CH}_3\text{C}(\text{O})\text{OH}$ ,  $\text{CF}_3\text{O}^-$  often reacts via clustering chemistry, i.e.,  $\text{CF}_3\text{O}^- + \text{HX} \rightarrow \text{CF}_3\text{O}^- \cdot \text{HX}$ .<sup>25</sup> While investigating the ion reaction chemistry of  $\text{CF}_3\text{O}^-$  with peroxyntic acid,  $\text{HNO}_4$  (which also reacts both by fluoride transfer and clustering), we discovered that  $\text{CF}_3\text{O}^-$  clustered efficiently with  $\text{H}_2\text{O}_2$ , which is a reagent (and impurity) in the synthesis of  $\text{HNO}_4$ . Further experimentation with additional hydroperoxides ( $\text{CH}_3\text{OOH}$ ,  $\text{CH}_3\text{C}(\text{O})\text{OOH}$ , and  $\text{HOCH}_2\text{OOH}$ ) showed that many other compounds of this type cluster efficiently with  $\text{CF}_3\text{O}^-$ .

The efficiency of the clustering of  $\text{CF}_3\text{O}^-$  with a particular  $\text{ROOH}$  is highly dependent on the water vapor mixing ratio. To quantify this dependence in the laboratory, we introduced a known quantity of  $\text{ROOH}$  into the flow tube and monitored instrument sensitivity as a function of flow tube humidity, which we controlled.

$\text{H}_2\text{O}_2$  was introduced to the humidity-controlled flow tube by flowing dry  $\text{N}_2$  over urea hydrogen peroxide (UHP) held at constant temperature. Constant outputs of other hydroperoxides came from temperature-controlled diffusion vials. PAA and UHP are available commercially (Sigma-Aldrich) while MHP<sup>32</sup> and HMHP<sup>33</sup> were synthesized in the laboratory, using established methods. While we had no incidents, extreme care must be taken synthesizing these peroxides as they have been known to explode unexpectedly.

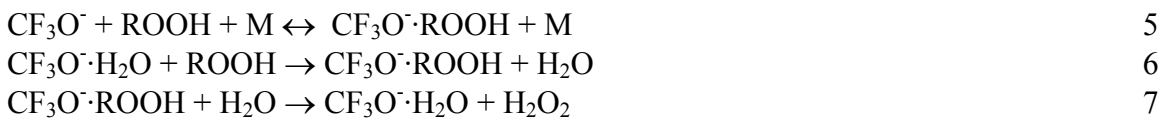
We controlled the humidity with mass flow controllers, adjusting the proportion of water vapor saturated air to dry zero air (Air Liquide) entering the flow tube. The saturated air was provided by a series of two atmospheric pressure (1013 hPa)  $\text{H}_2\text{O}$  bubblers submerged in a temperature controlled bath held at  $40^\circ\text{C}$ . After the second bubbler, the saturated air flowed through an orifice to reduce the pressure and avoid water condensation in the flow tube, even at high water vapor mixing ratios and reduced temperature. The measured rate of mass loss of the water in the double bubbler system was consistent with complete saturation of the air exiting the bubbler.

Figure 2:

Figure 2 illustrates mass scans in the region of the  $\text{CF}_3\text{O}^- \cdot \text{H}_2\text{O}_2$  cluster (119 amu). At high concentrations of  $\text{H}_2\text{O}$ , the  $\text{CF}_3\text{O}^-$  is present as  $\text{CF}_3\text{O}^- \cdot \text{H}_2\text{O}$  (103 amu),  $\text{CF}_3\text{O}^- \cdot (\text{H}_2\text{O})_2$  (121 amu), and higher clusters -  $\text{CF}_3\text{O}^- \cdot (\text{H}_2\text{O})_n$ . This decreases the sensitivity to  $\text{H}_2\text{O}_2$  (and other peroxides) and increases the backgrounds due to the hydrolysis of  $\text{CF}_3\text{O}^-$  by  $\text{H}_2\text{O}$  to  $\text{F}^- \cdot (\text{H}_2\text{O})_n$  ions.

While the thermodynamics of the reaction mechanism are beyond the scope of this paper, the following reactions are likely responsible for the changing sensitivity in response to varying  $[\text{H}_2\text{O}]$ :

Figure 3:



For  $\text{H}_2\text{O}_2$ , reaction 5 (forward) is somewhat slower than 6, so the sensitivity improves as  $[\text{H}_2\text{O}]$  increases to 0.1% before decreasing at higher water mixing ratios. For other peroxides (e.g., MHP), the sensitivity decreases with increasing  $\text{H}_2\text{O}$  for all  $\text{H}_2\text{O}$  concentrations. The ratio of reaction 7 to 6 sets how quickly the sensitivity declines with  $[\text{H}_2\text{O}]$ . For relatively strong clusters (e.g.,  $\text{H}_2\text{O}_2\text{-CF}_3\text{O}^\cdot$  or  $\text{PAA}\text{-CF}_3\text{O}^\cdot$ ) the falloff is less steep than for weaker ones (e.g.,  $\text{CH}_3\text{OOH}\text{-CF}_3\text{O}^\cdot$  or  $\text{CH}_3\text{CH}_2\text{OOH}\text{-CF}_3\text{O}^\cdot$ ). Thus, for accurate quantification, each individual compound must be calibrated separately; in addition, the curves shown in Figure 2 will be specific to the conditions in the ion flow tube (pressure, temperature, and interaction time). The heat of formation of  $\text{CF}_3\text{O}^\cdot\text{-H}_2\text{O}_2$  has not been measured, but the binding energy is greater than that of  $\text{CF}_3\text{O}^\cdot\text{-H}_2\text{O}$  ( $51 \text{ kJ mol}^{-1}$ )<sup>30</sup>, as evidenced by reaction 6. *Ab initio* calculations and thermodynamic discussions of the clustering chemistry will be addressed in a separate paper.

## 4. Field Operation

### 4.1 Calibration

In addition to the laboratory calibrations, the instrument was calibrated hourly during flight using standard additions of gas phase  $\text{H}_2\text{O}_2$ ,  $\text{HNO}_3$ ,  $\text{HC(O)OH}$ , and  $\text{H}_3\text{CC(O)OH}$  to the flow tube. The nitric acid and organic acid standards are isotopically labeled and evolve from permeation tubes held at constant temperature.<sup>34</sup> The  $\text{H}_2\text{O}_2$  calibration standard is produced by flowing dry  $\text{N}_2$  over UHP held at a constant temperature of  $0^\circ \text{C}$  in a glass U-tube. At  $0^\circ \text{C}$  UHP has a  $\text{H}_2\text{O}_2$  vapor pressure of  $1.4 \times 10^{-3} \text{ hPa}$  (determined by collecting the output in water and analyzing with a standard colorimetric technique (Bioxytech  $\text{H}_2\text{O}_2$ -560, Bio-Stat Research). Maintaining the pressure (2000 hPa) and flow (80 sccm) constant, one produces a standard of 700 ppbv  $\text{H}_2\text{O}_2$ . A fraction of this flow (22 sccm) is injected into the flow tube and diluted by the either scrubbed ambient air, or zero air (1800 sccm) to give a concentration of 8 ppbv  $\text{H}_2\text{O}_2$  in the ion flow tube. This source produces a constant ( $\pm 10\%$ ) mass flow of  $\text{H}_2\text{O}_2$  over several months, without need to refresh the UHP. The sensitivity for other species (e.g. HCN and PAA) was inferred from laboratory determination of the relative calibration factors for these compounds compared to the standards used in flight.

### 4.2 Water sensitivity

Accounting for the change in sensitivity with variation in the water vapor mixing ratio is critical for accurate measurements. During INTEX-NA, the ion flow tube air was essentially undiluted ambient air. Water vapor mixing ratios varied from more than 3% to as low as 10 ppmv resulting in very large changes in the sensitivity for all analytes. We account for these changes in sensitivity by using a combination of the

periodic calibrations and measurements of the ambient H<sub>2</sub>O mixing ratio by a separate instrument on the DC-8 - the tunable diode laser hygrometer.<sup>35</sup> In the future, we plan to use a 1:4 mix of ambient air to dry nitrogen to avoid H<sub>2</sub>O mixing ratios greater than 1%. Above 1% humidity, we observe substantial hydrolysis of our reagent ion. The hydrolysis of the reagent ion yields many product ions which clutter the mass spectrum.

### 4.3 Backgrounds

Even in the absence of analytes, ion signals are often present at masses of interest. These arise from interferences from mass analogs as well as H<sub>2</sub>O clusters of other ions present in the flow. We use two methods in flight to estimate these background signals. In the first, ambient air is “scrubbed” by passing it through a two-stage filter composed of (1) alumina pellets coated with palladium (Sigma-Aldrich) and (2) nylon wool coated with sodium bicarbonate before entering the flow tube. This filter quantitatively removes H<sub>2</sub>O<sub>2</sub> and organic peroxides (as well as most acids). In the second, high purity zero air from a cylinder (Air Liquide) is added to the flow tube instead of ambient air. Neither method is ideal. Although the filter scrubs targeted analytes from the air, it may also scrub the species which cause mass analog background signals. The bottled air measures the instrument background signal, but does not give any information about mass analog backgrounds in ambient air. Also, both methods, generally, alter the humidity in the flow tube which, as discussed above, directly affects the sensitivity for these gases.

Fortunately, for many analytes, including H<sub>2</sub>O<sub>2</sub> and PAA, these backgrounds tend to be relatively constant (at a given water vapor concentration). For CH<sub>3</sub>OOH, backgrounds at mass 133 (Si(CH<sub>3</sub>)<sub>2</sub>F<sub>3</sub><sup>-</sup>·H<sub>2</sub>O) coupled with low sensitivity due to high water concentrations in the flow tube prevented us from making make usable measurements of this compound during INTEX-NA (see table S-1 for a summary of sensitivities and backgrounds).

### 4.4 Measurement of Additional Compounds using CF<sub>3</sub>O<sup>-</sup>

In addition to its clustering with ROOH, CF<sub>3</sub>O<sup>-</sup> clusters efficiently with other compounds that have historically been difficult to detect and quantify. During INTEX-NA, our instrument measured HCN and HNO<sub>3</sub> as well as H<sub>2</sub>O<sub>2</sub> and PAA, while organic acids, though quantifiable in principle, could not be measured effectively due to background issues. In addition, preliminary work in our laboratory demonstrates that many of the products of isoprene oxidation can be measured with high sensitivity using CF<sub>3</sub>O<sup>-</sup> clustering chemistry. These include isoprene-hydroxy-hydroperoxide, isoprene-hydroxy-nitrate, and hydroxy-acetone. Additional lab tests have confirmed this method to be sensitive for measuring compounds of the form R-CH(OOH)CH<sub>2</sub>(OH), R-C(O)CH<sub>2</sub>-OH, and R-C(ONO<sub>2</sub>)C-OH. A paper describing these experiments on isoprene oxidation products will be forthcoming.

## 5. Comparison with HPLC method

During the INTEX-NA field campaign, the CIMS instrument measured H<sub>2</sub>O<sub>2</sub> and PAA with an approximate 7% and 3% duty cycle, respectively. The remainder of the time

instrument measured other compounds (e.g., HNO<sub>3</sub> and HCN), backgrounds, standards, the reagent ion, and its water clusters, which are necessary for data reduction. This field experiment provided over 28 hours of direct comparison of this new peroxide technique with observations from the University of Rhode Island HPLC-Fluorescence instrument.<sup>11</sup> These flights spanned conditions from the polluted boundary layer to the remote free troposphere and lower stratosphere.

Figure 5 shows the comparison for H<sub>2</sub>O<sub>2</sub> and PAA from these two instruments. Overall, agreement is quite good for both species. 89% and 92% of the observations for H<sub>2</sub>O<sub>2</sub> and PAA, respectively, lie within experimental uncertainty. The correlation for the PAA comparison ( $r^2 = 0.60$ ) is somewhat less than for H<sub>2</sub>O<sub>2</sub> ( $r^2 = 0.82$ ), possibly due to the fact that: 1) there were 45% fewer comparisons for PAA than H<sub>2</sub>O<sub>2</sub>; 2) The dynamic range was significantly smaller for PAA than H<sub>2</sub>O<sub>2</sub>; and 3) the HPLC detection limit was significantly higher for PAA than for H<sub>2</sub>O<sub>2</sub>. The uncertainty in CIMS measurements during INTEX-NA were ~ 35% for H<sub>2</sub>O<sub>2</sub> and ~ 35% for PAA, and are primarily determined by uncertainties in backgrounds and our water sensitivity determination. Agreement at both low and high humidity demonstrates that our parameterization of the humidity dependence of the instrument's sensitivity is adequate for water mixing ratios of less than 10 ppmv up to 2% (see figure S-1).

Figure 4 :

## 6. Conclusions and Summary

CIMS using CF<sub>3</sub>O<sup>-</sup> as a reagent ion has been successfully demonstrated to measure hydroperoxides H<sub>2</sub>O<sub>2</sub> and PAA with good sensitivity (25 pptv for H<sub>2</sub>O<sub>2</sub>, 25 pptv for PAA) and time resolution (< 1s). This fast technique will enhance studies of heterogeneous air masses, and is particularly useful for airborne sampling. High temporal resolution aircraft measurements of hydroperoxides will contribute to the study of many important atmospheric processes including convective transport, cloud processing, and aerosol aging. Further development of this method should increase its applicability to other important compounds, such as CH<sub>3</sub>OOH, HMHP, and the products of isoprene oxidation.

## Acknowledgements

We thank Dan O'Sullivan, Julie Snow, Haiwei Shen, and Brian Heikes for allowing us to show their H<sub>2</sub>O<sub>2</sub> and PAA data prior to publication. We thank Norton Allen and James Oliver for their assistance in the preparation of the CIMS instrument for the DC-8. We thank Suresh Dhaniyala for his assistance in the design of the inlet. Funding for this work was provided by a grant from the National Aeronautics and Space Administration (NAG: NNG04GA59G). We also thank the EPA-STAR Fellowship Program (FP916334012) and the NSF Graduate Research Fellowship program for providing support for the authors.

## References:

- (1) Wennberg, P. O.; Hanisco, T. F.; Jaegle, L.; Jacob, D. J.; Hintsa, E. J.; Lanzendorf, E. J.; Anderson, J. G.; Gao, R. S.; Keim, E. R.; Donnelly, S. G.; Del Negro, L. A.; Fahey, D. W.; McKeen, S. A.; Salawitch, R. J.; Webster, C. R.; May, R. D.; Herman, R. L.; Proffitt, M. H.; Margitan, J. J.; Atlas, E. L.; Schauffler, S. M.; Flocke, F.; McElroy, C. T.; Bui, T. P. *Science* **1998**, *279*, 49-53.
- (2) Jaegle, L.; Jacob, D. J.; Brune, W. H.; Faloona, I.; Tan, D.; Heikes, B. G.; Kondo, Y.; Sachse, G. W.; Anderson, B.; Gregory, G. L.; Singh, H. B.; Poeschel, R.; Ferry, G.; Blake, D. R.; Shetter, R. E. *J Geophys Res D: Atmos* **2000**, *105*, 3877-3892.
- (3) Penkett, S. A.; Jones, B. M. R.; Brice, K. A.; Eggleton, A. E. *J. Atmos. Environ.* **1979**, *13*, 123-137.
- (4) Claeys, M.; Wang, W.; Ion, A. C.; Kourtschev, I.; Gelencser, A.; Maenhaut, W. *Atmos. Environ.* **2004**, *38*, 4093-4098.
- (5) Gab, S.; Turner, W. V.; Wolff, S.; Becker, K. H.; Ruppert, L.; Brockmann, K. J. *Atmos. Environ.* **1995**, *29*, 2401-2407.
- (6) Madronich, S., *Personal communication*, NCAR, 2005.
- (7) Kok, G. L.; Heikes, B. G.; Lind, J. A.; Lazrus, A. L. *Atmos. Environ.* **1989**, *23*, 283-283.
- (8) Lee, M. H.; Heikes, B. G.; O'Sullivan, D. W. *Atmos. Environ.* **2000**, *34*, 3475-3494.
- (9) Heikes, B. G.; Kok, G. L.; Walega, J. G.; Lazrus, A. L. *J Geophys Res D: Atmos* **1987**, *92*, 915-931.
- (10) Penkett, S. A.; Bandy, B. J.; Reeves, C. E.; McKenna, D.; Hignett, P. *Faraday Discuss.* **1995**, 155-174.
- (11) Lee, M.; Noone, B. C.; Osullivan, D.; Heikes, B. G. *J. Atmos. Ocean. Technol.* **1995**, *12*, 1060-1070.
- (12) Slemr, F.; Harris, G. W.; Hastie, D. R.; Mackay, G. I.; Schiff, H. I. *J Geophys Res D: Atmos* **1986**, *91*, 5371-5378.
- (13) Kormann, R.; Fischer, H.; Gurk, C.; Helleis, F.; Klupfel, T.; Kowalski, K.; Konigstedt, R.; Parchatka, U.; Wagner, V. *Spectroc. Acta Pt. A-Molec. Biomolec. Spectr.* **2002**, *58*, 2489-2498.
- (14) Fahey, D. W.; Gao, R. S.; Carslaw, K. S.; Kettleborough, J.; Popp, P. J.; Northway, M. J.; Holecek, J. C.; Ciciora, S. C.; McLaughlin, R. J.; Thompson, T. L.; Winkler, R. H.; Baumgardner, D. G.; Gandrud, B.; Wennberg, P. O.; Dhaniyala, S.; McKinney, K.; Peter, T.; Salawitch, R. J.; Bui, T. P.; Elkins, J. W.; Webster, C. R.; Atlas, E. L.; Jost, H.; Wilson, J. C.; Herman, R. L.; Kleinbohl, A.; von Konig, M. *Science* **2001**, *291*, 1026-1031.
- (15) Furutani, H.; Akimoto, H. *J Geophys Res D: Atmos* **2002**, *D1-D2*, 4016.
- (16) Miller, T. M.; Ballenthin, J. O.; Meads, R. F.; Hunton, D. E.; Thorn, W. F.; Viggiano, A. A.; Kondo, Y.; Koike, M.; Zhao, Y. J. *J Geophys Res D: Atmos* **2000**, *105*, 3701-3707.
- (17) Neuman, J. A.; Huey, L. G.; Dissly, R. W.; Fehsenfeld, F. C.; Flocke, F.; Holecek, J. C.; Holloway, J. S.; Hubler, G.; Jakoubek, R.; Nicks, D. K.; Parrish,

- D. D.; Ryerson, T. B.; Sueper, D. T.; Weinheimer, A. J. *J Geophys Res D: Atmos* **2002**, *D20*, 4436.
- (18) Zondlo, M. A.; Mauldin, R. L.; Kosciuch, E.; Cantrell, C. A.; Eisele, F. L. *J Geophys Res D: Atmos* **2003**, *D20*, 8793.
- (19) Marcy, T. P.; Gao, R. S.; Northway, M. J.; Popp, P. J.; Stark, H.; Fahey, D. W. *Int. J. Mass Spectrom.* **2005**, *243*, 63-70.
- (20) Reiner, T.; Mohler, O.; Arnold, F. *J Geophys Res D: Atmos* **1998**, *103*, 31309-31320.
- (21) Cantrell, C. A.; Edwards, G. D.; Stephens, S.; Mauldin, L.; Kosciuch, E.; Zondlo, M.; Eisele, F. *J Geophys Res D: Atmos* **2003**, *D6*, 8371.
- (22) Viggiano, A. A.; Hunton, D. E.; Miller, T. M.; Ballenthin, J. O. *J Geophys Res D: Atmos* **2002**, *D5*, 8304.
- (23) Nowak, J. B.; Davis, D. D.; Chen, G.; Eisele, F. L.; Mauldin, R. L.; Tanner, D. J.; Cantrell, C.; Kosciuch, E.; Bandy, A.; Thornton, D.; Clarke, A. *Geophys. Res. Lett.* **2001**, *28*, 2201-2204.
- (24) Mauldin, R. L.; Cantrell, C. A.; Zondlo, M. A.; Kosciuch, E.; Ridley, B. A.; Weber, R.; Eisele, F. E. *J Geophys Res D: Atmos* **2003**, *D4*, 8366.
- (25) Amelynck, C.; Schoon, N.; Arijs, E. *Int. J. Mass Spectrom.* **2000**, *203*, 165-175.
- (26) Nowak, J. B.; Huey, L. G.; Eisele, F. L.; Tanner, D. J.; Mauldin, R. L.; Cantrell, C.; Kosciuch, E.; Davis, D. D. *J Geophys Res D: Atmos* **2002**, *D18*, 4363.
- (27) Slusher, D. L.; Pitteri, S. J.; Haman, B. J.; Tanner, D. J.; Huey, L. G. *Geophys. Res. Lett.* **2001**, *28*, 3875-3878.
- (28) Messer, B. M.; Stielstra, D. E.; Cappa, C. D.; Scholtens, K. W.; Elrod, M. J. *Int. J. Mass Spectrom.* **2000**, *197*, 219-235.
- (29) Warneke, C.; Holzinger, R.; Hansel, A.; Jordan, A.; Lindinger, W.; Poschl, U.; Williams, J.; Hoor, P.; Fischer, H.; Crutzen, P. J.; Scheeren, H. A.; Lelieveld, J. *J. Atmos. Chem.* **2001**, *38*, 167-185.
- (30) Amelynck, C.; Van Bavel, A. M.; Schoon, N.; Arijs, E. *Int. J. Mass Spectrom.* **2000**, *202*, 207-216.
- (31) Huey, L. G.; Villalta, P. W.; Dunlea, E. J.; Hanson, D. R.; Howard, C. J. *J. Phys. Chem.* **1996**, *100*, 190-194.
- (32) Vaghjiani, G. L.; Ravishankara, A. R. *J. Phys. Chem.* **1989**, *93*, 1948-1959.
- (33) Marklund, S. *Acta Chem. Scand.* **1971**, *25*, 3517.
- (34) Washenfelder, R. A.; Roehl, C. M.; McKinney, K. A.; Julian, R. R.; Wennberg, P. O. *Rev. Sci. Instrum.* **2003**, *74*, 3151-3154.
- (35) Podolske, J. R.; Sachse, G. W.; Diskin, G. S. *J Geophys Res D: Atmos* **2003**, *D20*, 8792.



Figure 2: The sensitivity to  $\text{H}_2\text{O}_2$  (mass 119) depends on water (stars = 10000 ppmv  $\text{H}_2\text{O}$ , circles = 100 ppmv  $\text{H}_2\text{O}$ ) due to reduced sensitivity and increase in the background. For the mass scans illustrated here, the  $\text{H}_2\text{O}_2$  mixing ratio is 5000 pptv (closed stars), 500 pptv (closed circles), or < 50 pptv (open symbols).

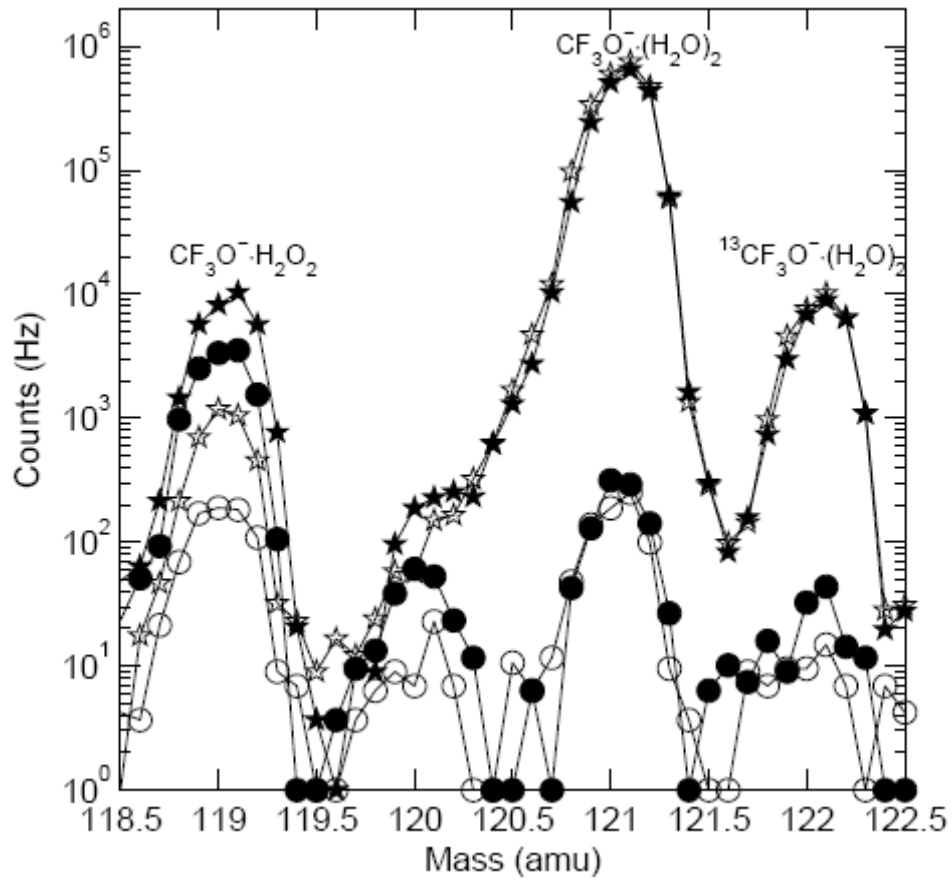
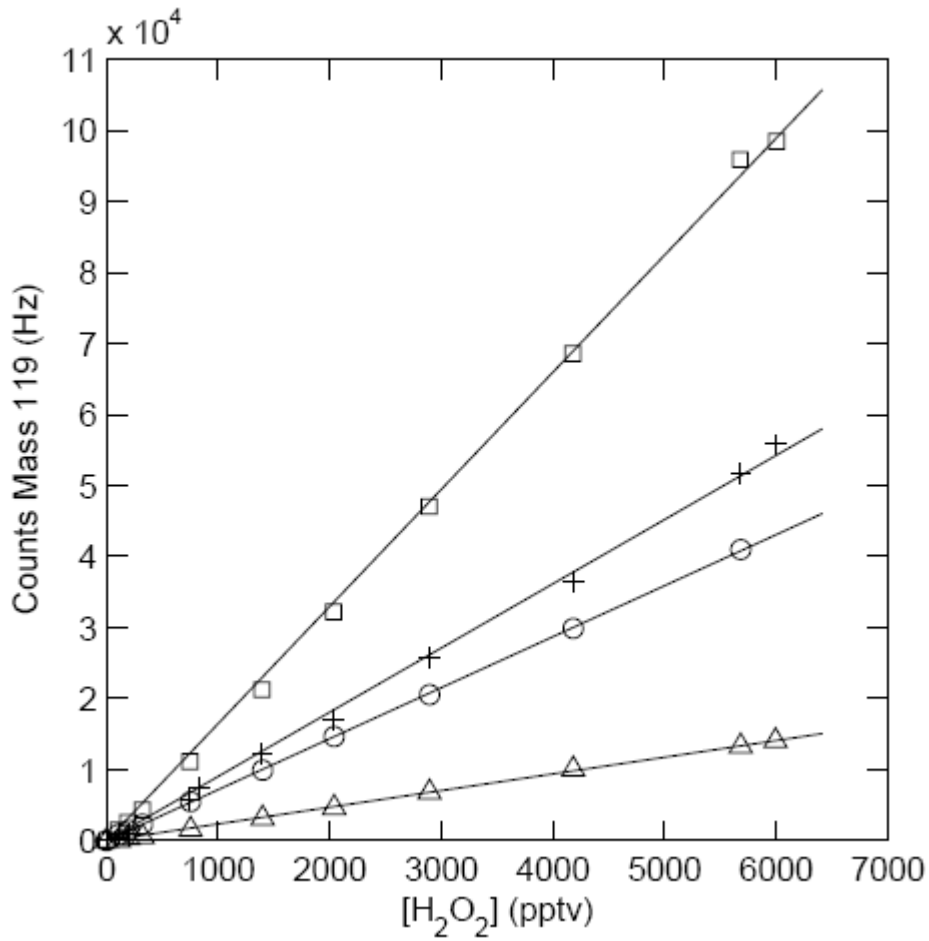


Figure 3: A. Mass 119 signal as a function of  $[H_2O_2]$  for several  $H_2O$  concentrations: plus  $[H_2O] = 10\text{ppmv}$ , square  $[H_2O] = 1000\text{ ppmv}$ , circle  $[H_2O] = 5000\text{ ppmv}$ , triangle  $[H_2O] = 10000\text{ ppmv}$ . B. Normalized signal for mass 119 (solid-thick), mass 161 (dotted), mass 112 (dashed), mass 82 (dash-dot), and mass 133 (solid-thin) signal as a function of  $[H_2O]$ , for a while adding a constant amount of  $H_2O_2$ , PAA, HCN,  $HNO_3$ , and MHP, respectively.

A.



B.

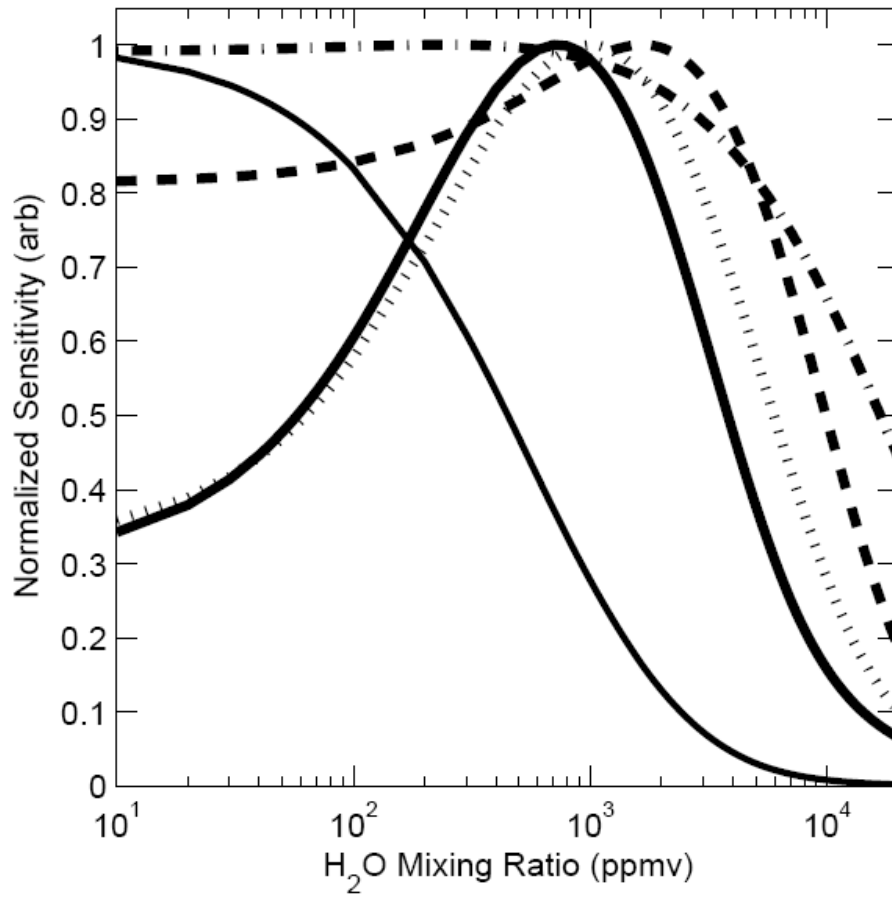
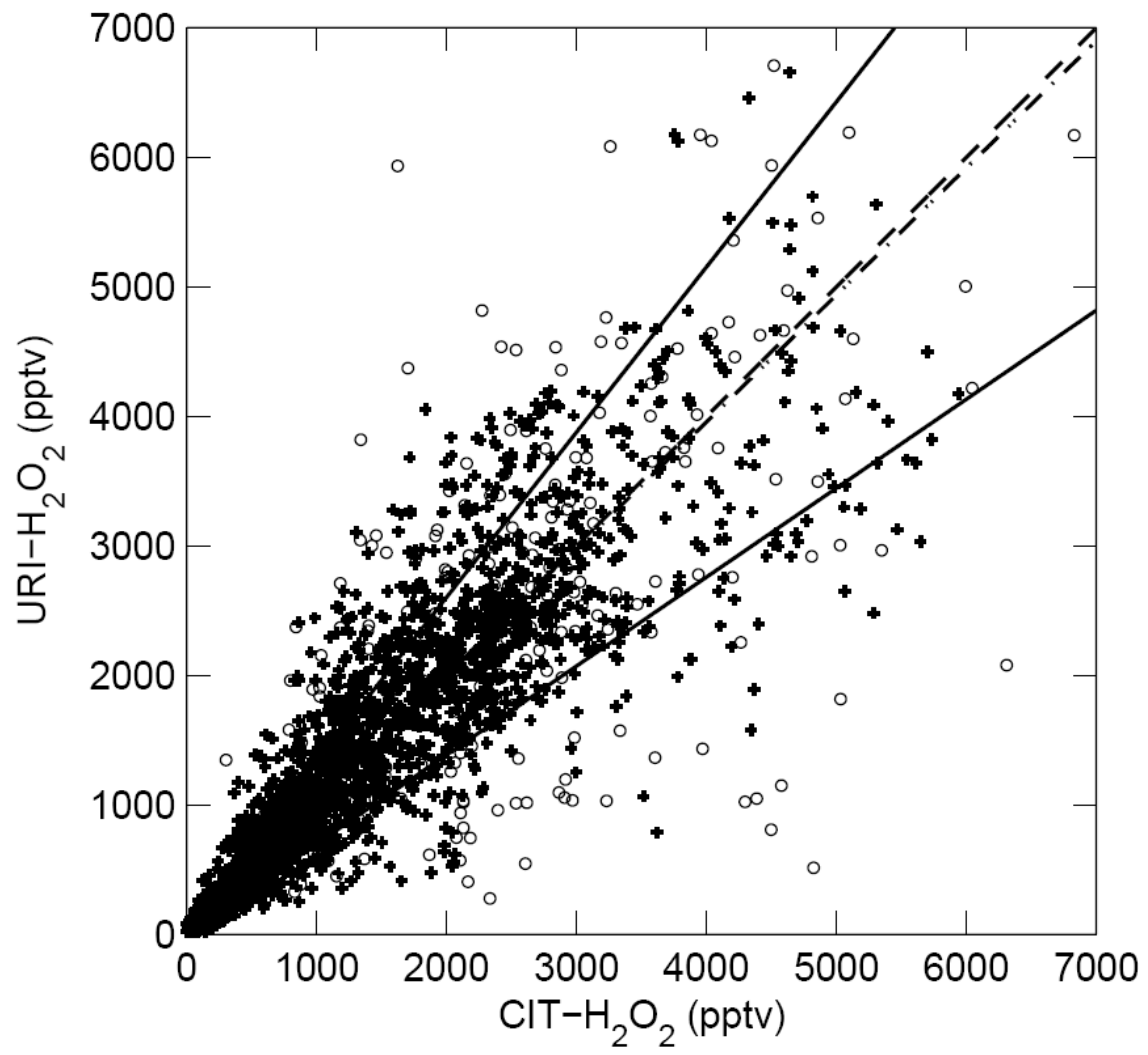


Figure 4: A) University of Rhode Island H<sub>2</sub>O<sub>2</sub> vs Caltech CIMS H<sub>2</sub>O<sub>2</sub> both measured aboard NASA DC-8 during INTEX-NA. 89% of the measurements agree within uncertainties after averaging the faster measurement to the slower time base for a total of 2793 comparable observations. Solid lines are error limits about dash-dot line, the dash-dot line. The data were filtered (open circles-rejected (~8%), plus symbols (+)-accepted (~91%)) using a first derivative cut off (~17 pptv/s) in the time domain for each set of data to remove outliers. The reasons for using the derivative cutoff are twofold: 1) there are errors associated with averaging the fast time-base to the slower one, and these are more prevalent when the analyte concentration is changing rapidly and 2) the Caltech CIMS measurements occasionally were affected by short periods of electronic noise. Both error sources are captured by the derivative cutoff. The dash-dot line is the Matlab© robust fit to filtered data (+) with  $m=0.98$ ,  $b= 32$  pptv and  $r^2=0.82$ , and the dashed line is 1-1 line. B) Same comparison as panel A, but for PAA measurements. 92% of measurements lie within uncertainties for the 1504 comparable observations. The first derivative cutoff (~6 pptv/s) removed 1% of the data. Solid lines are error limits about dash-dot line, the dash-dot line is Matlab© robust fit to the filtered data (+) with  $m=0.69$ ,  $b= 56$  pptv, and  $r^2=0.60$ . The dashed line is 1-1 line.

A.



B.

